IEEE Access
Multidisciplinary | Rapid Review | Open Access Journal

Received 22 February 2024, accepted 25 March 2024, date of publication 5 April 2024, date of current version 16 April 2024.

Digital Object Identifier 10.1109/ACCESS.2024.3385435

RESEARCH ARTICLE

On-Device Intelligence for AI-Enabled Bio-Inspired Autonomous Underwater Vehicles (AUVs)

ARYAN ANAND[1], (Member, IEEE), M YUVA BHARATH[2], PRABHA SUNDARAVADIVEL[1], (Member, IEEE), J. PREETHA ROSELYN[3], (Senior Member, IEEE), AND R. ANNIE UTHRA[3]

[1]Department of Electrical and Computer Engineering, The University of Texas at Tyler, Tyler, TX 75701 USA
[2]AR4 Tech Pvt. Ltd., Coimbatore 641107, India
[3]SRM Institute of Science and Technology, Kattankulathur, Chennai, Tamil Nadu 603203, India

Corresponding author: J. Preetha Roselyn (preethaj@srmist.edu.in)

This work was supported in part by the University of Texas System STAR Award under Grant T231424B, in part by the University of Texas at Tyler Open Access Funding Initiative, and in part by the Sri Ramasamy Memorial (SRM) Institute of Science and Technology.

ABSTRACT This paper introduces an innovative approach to underwater exploration by integrating Artificial Intelligence (AI) into Autonomous Underwater Vehicles (AUVs). This collaboration between AI and biomimicry marks a new era for AUVs, enabling them to emulate marine creatures' graceful and efficient movements. By infusing AI capabilities into AUVs, AUVs are empowered to learn and adapt, making autonomous real-time decisions without human intervention. This dynamic integration equips AUVs to effectively navigate complex underwater terrains, evade obstacles, and seamlessly interact with marine life. Inspired by the remarkable propulsion mechanisms found in marine organisms, this work proposes a pioneering propulsion system tailored for AUVs. Taking cues from the locomotion of creatures like cuttlefish, the biomechanics is translated into a robotic propulsion system. The result is a fluid and energy-efficient propulsion method that mitigates the harmful effects of cavitation, thereby reducing noise pollution and minimizing disruption to marine ecosystems. This research evaluates the performance of on-device AI models for analyzing the sensing environment around the AUV and taking real-time images. This automated sensing and navigation method can help the AUVs independently navigate to the desired location along the water table. The propulsion is achieved by building a crankshaft mechanism and a unified mechanical design to convert rotational motion from a motor into a sinusoidal wave motion to replicate the cuttlefish locomotion pattern. The proposed underwater vehicle, Aquabot, is designed using Fusion 360 simulation and ANSYS software. The results demonstrate the accuracy and efficiency of the autonomous underwater vehicle based on the environmental conditions, thus reducing energy consumption and enhancing aquatic vehicle efficiency.

INDEX TERMS Aquatic vehicle, propulsion system, object detection, bio-inspired, cuttle fish locomotion.

I. INTRODUCTION

Autonomous Underwater Vehicles (AUVs) can help map the climate, including monitoring several factors such as location, season, temperature, pressure, and water depth. AUVs are typically used for marine explorations, including oceanographic research, environmental monitoring, underwater mapping, and underwater inspections [1], [2], [3], [4], [5], [6], [7]. Conventional underwater data collection methods are through sondes and sampling systems that measure water quality parameters using circuit boards and calibrated sensors in enclosed PVC pipes. The existing underwater sensing frameworks are limited by being bulky, expensive, and requiring constant calibration.

In fresh or stagnant water bodies, the mobility of the AUV becomes challenging because of the uneven distribution of

The associate editor coordinating the review of this manuscript and approving it for publication was Zhongyi Guo.

the terrain's depth, salinity (usually less than 1%), temperature, and precipitation, which changes due to the regions where they occur. The dirt in every ounce of water increases in freshwater with less water movement. Analysing these microclimates can benefit the research in studying the underwater parameters that externally influence the habitats that flourish in the water ecosystem.

The AUVs are characterized by their *autonomy*, where pre-programmed instructions and on-board sensors are used to add some intelligence to the bot [8], [9], [10]; *mobility* in terms of propulsion systems and methods that can help them move through the water [11], [12], [13], [14]; *on-board sensors* and *communication protocols* that can help in collecting data and transmit them to the nearest station [15], [16], [17]; *size and shape* depending upon which the application of these AUVs are decided [18], [19], [20].

In such autonomous vehicles, researchers have explored the characteristics of thruster depth control design using PID (Proportional-Integral-Derivative) and LQR (Linear Quadratic Regulator) for AUVs [21]. Similarly, researchers have demonstrated how propellers in the low-frequency range can overlap and conceal the communication frequency band of marine mammals, impairing their basic life functions [22]. A comprehensive study exploring the fundamental principles governing diverse fish locomotion patterns, emphasizing distinct movement modes and navigation strategies, is presented in [23]. It particularly underscores the pivotal role of a robust spine in facilitating fast swimming, a cornerstone premise of aquatic mobility. Researchers in [24] presented an electrical propulsion system for an Autonomous Underwater Vehicle (AUV) and simulated its performance using MATLAB GUI. This study is focused on developing and simulating an electrical propulsion system for an unmanned underwater vehicle, with a particular emphasis on conducting real-time simulations to analyze speed variations to underlying physics principles. Traditional micro AUVs typically rely on thrusters for depth adjustments, leading to notable power consumption. Introducing a variable buoyancy system is explored to address this challenge and enhance energy efficiency. In [25], the authors provide insights into this system, encompassing electromechanical and electrohydraulic components.

Moreover, the unveiling of a bio-inspired soft robotics AUV in 2020 [26] underscores the growing interest in alternative propulsion mechanisms. Conventional thruster-based AUVs have raised concerns due to potential risks to marine life resulting from cavitation generated by fast-moving blades. Our research proposes an innovative propulsion system inspired by cuttlefish movement to address this concern. This system adopts a unified mechanical design to convert rotational motion into sinusoidal wave motion, offering a novel approach to propulsion utilizing sine wave movements.

While the research in underwater propulsion systems shows promise, several research studies have emphasized the importance of on-device sensors, particularly cameras. Recent works in underwater object detection have focused on leveraging deep learning techniques to improve the accuracy and efficiency of detection algorithms. Deep neural networks, such as the various YOLO (You Only Look Once) architectures, have demonstrated remarkable performance in detecting and localizing objects in underwater imagery. This proposed approach showcases superiority over previous methods in recognizing underwater objects, as demonstrated through comparisons with various models.

Ayob et al. [27] analyze the pruned neural network architectures for underwater object detection. Their study scrutinizes the efficacy of pruning techniques in streamlining model complexity and computational demands while maintaining detection performance. Thuan et al. [28] provide an in-depth exploration of the evolutionary journey of the YOLO (You Only Look Once) algorithm, with a specific focus on the YOLOv5 model. In their research, the authors discuss the key advancements and refinements introduced across various iterations of the YOLO algorithm, elucidating the strengths and limitations inherent in the YOLOv5 model. Xu et al. [29] concentrate on utilizing deep learning methodologies for underwater fish detection within underwater contexts. Their work introduces a deep learning framework tailored for identifying and localizing fish species in underwater environments. Miao Yang et al. [30] comprehensively analyze multiple underwater picture enhancement techniques, encompassing both traditional and state-of-the-art approaches. Their survey identifies the challenges in aquatic cinematography, including color distortion, low visibility, and noise, exploring strategies such as dehazing, image fusion, contrast enhancement, and color correction. The review also discusses the metrics utilized to assess the efficacy of these enhancement strategies. Kim et al. [31] extensively examine picture and video dehazing methods specifically tailored for underwater scenarios. Addressing challenges arising from light attenuation, backscatter, and color distortion in aquatic environments, the review surveys a range of dehazing techniques, including depth estimation-based methods, multi-image fusion, and single-image dehazing. These methods aim to alleviate visibility issues caused by light absorption and dispersion, posing challenges for information acquisition and marine research. Redmon et al. [32] introduce the YOLO algorithm for real-time single object detection. Their work presents an architecture that divides input images into a grid, predicting bounding boxes and probabilities for each class. YOLO's ability to achieve competitive detection accuracy at impressive real-time speeds, as demonstrated in the literature, renders it suitable for applications requiring rapid and efficient object detection.

To address these concerns, in our research max-rgb and shades of grey methods are combined with Convolution Neural Network (CNN) techniques to enhance underwater vision. The weak conditions identified using CNN are employed with image processing to generate an illuminance map. A deep CNN approach is suggested for underwater object detection and classification. Two revised strategies to modify the deep

CNN structure are proposed to cater to underwater vision properties. These strategies involve adding down sampling and convolution layers, producing a more effective detection map.

The main contributions of this paper are as follows:

- Design of AI empowered and bio inspired autonomous underwater vehicle which incorporates propulsion mechanisms inspired by cuttle fish.
- To achieve variable buoyancy system that enables the vehicle to achieve neutral buoyancy at specific depths.
- To build a prototype of Aquabot which includes manufacturing parts of bio-inspired AUV, and the addition of electronics like sensors, actuators and battery systems.
- AI based object detection and intelligent navigation process in developed AUV using intelligent models like CNN incorporating adding down sampling and convolution layers and is deployed in real time processors along with aquabot.

II. CONVERGENCE OF AI AND BIOMIMICRY

The cuttlefish generates motion in a *catamaran* pattern. It has two sets of fins attached parallel to each other, generating a sinusoidal wave pattern when the fish is in motion. The agility of these sinusoidal waves can enable the fish to move frontward, backward, or sideways - depending on the direction of the sine wave. If both sine waves propagate in the same direction, the fish moves forward; if both sine waves propagate in the opposite direction, the fish moves backward; and if they alternately move in the opposite (clockwise and anticlockwise) direction, this can enable the power to change the direction easily.

The individual, discrete sine-wave-based fins also help prevent the fish's body from being disturbed when in motion. This eliminates the disadvantage caused by the shark's locomotion affecting the camera's stability, shown in Fig 1. Thus, the cuttlefish is ultimately chosen for the AUV's motion.

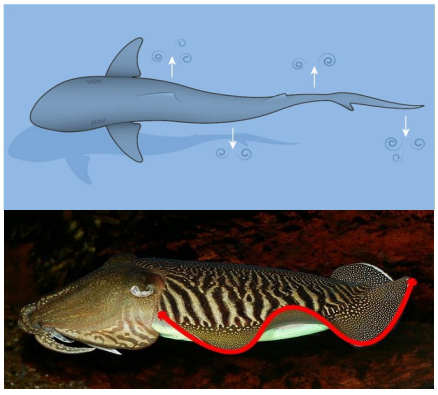

FIGURE 1. Locomotion of shark and cuttlefish.

In addition, Marine animals often use Variable buoyancy mechanisms to change their depth efficiently, for example Bony fish utilize swim bladders to regulate buoyancy by adjusting gas levels, while marine mammals like whales and dolphins rely on specialized lungs and circulatory systems to manage oxygen and blood flow during deep dives. Additionally, some species, such as sharks and rays, manipulate the oil content in their liver to control buoyancy. In current technical terms, modern AUVs achieve buoyancy control using a Variable Buoyancy System(VBS). The motivation behind enhancing Aquabot's capabilities with real-time interaction and artificial intelligence involves a comprehensive exploration of automation through deep learning and machine learning approaches. To implement this algorithm, the proposed algorithm is deployed onto NVIDIA's high-performance computation-enabled device, Jetson Nano (using the 4GB developer kit), and integrated with a high-quality camera for real-time functionality. Water's absorption and dispersion effects further exacerbate the challenges underwater visibility poses. Underwater cameras often yield images with poor contrast, uneven illumination, blurring, noise, and other distortions. Underwater object detection and the development of autonomous underwater vehicles have garnered significant attention in recent years. This work has concentrated on the deployment of CNN based intelligent algorithms for underwater object detection for the Aquabot which makes the system intelligent and indigenous under the marine environment.

III. DESIGN AND MODELING OF THE PROPOSED SYSTEM

The proposed AUV consists of controllability and maneuverability in 3 Degrees of Freedom (DoF). The Isometric view of AUV and its 3-axis model in the Body frame with reference to the Earth frame, is shown in Fig 2. The AUV is stable in Roll "Φ", Pitch "θ", and Sway "v" axes and the vehicle can be precisely controlled in Surge "u", Heave "w" (Two DoF in Translational direction), and Yaw "ψ" motions (1 DoF in Rotational). These 3 DoFs are required to mimic the locomotion of Cuttlefish. The Surge and Yaw motions are attained using two sets of fins, where when both fins travel in the same directions i.e. pushing water pockets under sine-wave-like curves in the same direction, gives positive or negative Surge control, and when both fins travel in the alternate directions i.e. pushing water pockets under sine-wave-like curves in the opposite direction, gives positive or negative Yaw control. The Heave motion is achieved by a Variable buoyancy system to change depth or hover at a certain depth by attaining neutral buoyancy.

The cuttlefish's locomotion for surge and yaw control is achieved by building a crankshaft mechanism and unified mechanical design to convert rotational motion from a motor into a sinusoidal wave motion. In this design, a sliding and angular crankshaft mechanism is made where the crank pin has a deflection of 25 to 75-degree crank angle in which 25 degrees gives more higher amplitude sinusoidal wave but weighs more. At 75 degree angle, a low amplitude sinusoidal wave is achieved with less weight. Also, the lower crank angle gives a smoother sine-like wave. In cuttlefish, each side of their body has fins with one full sine wave and a half sine

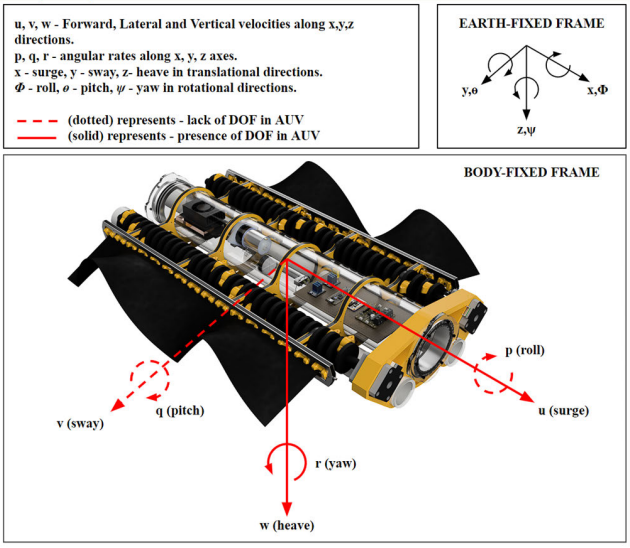

FIGURE 2. Isometric view of AUV and 3-axis model showing multi-DoF.

wave. For the proposed AUV, 2 sine waves can provide the required thrust and stability.

The required fin should produce two full sine waves to be driven by cranks and the number of cranks (N) needed to drive the fins. Equation 1 is formed where N is the number of cranks needed, and θ_{crank} is the crank angle.

$$\mathrm{N} = 2 \times \frac{360^\circ}{\theta crank} \tag{1}$$

The crank angle defines how much the fin will resemble a sine wave. The smaller the value of θ_{crank}, the more well-defined the wave shape shown in Fig 3.

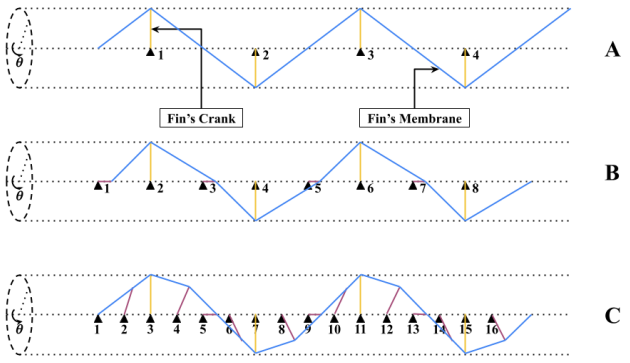

FIGURE 3. Fins membrane trajectory with respect to number of crank (rays). (A) θcrank 180°, (B) θcrank 90°, (C) θcrank 45°.

Hence, an optimal angle of 45 degrees with a total number of 16 cranks in each fin is used in this propulsion system which achieves optimum amplitude and wavelength that matches the motion of real cuttlefish fins shown as a blue colour sine-like wave in Fig 3 and Fig 4 which matches with a wave pattern in Fig 1. The designed angular and cylindrical sliding shafts are attached to silicon molded fins to develop the cuttlefish propulsion system.

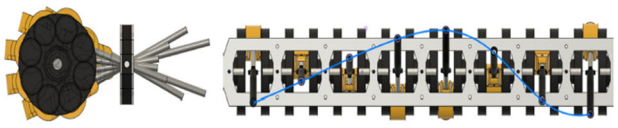

FIGURE 4. Crankshaft degree mechanism.

The working principle of the proposed propulsion system in crank slider 3rd inversion. In fig 5, the setup demonstrates the crank slider mechanism used in the propulsion, where the red bar CA is 15 mm long and the freedom of rotation of 360°, the magenta bar CH is 50 mm and grounded, the green bar AB is 75 mm long calculate in (2) and can rotate partially and slides through H (hinge-slider pin). The blue circle at point A has a 10 mm diameter and the circle at C is also of 10 mm diameter. The shaft circle is 40 mm in diameter shown in Fig 5.

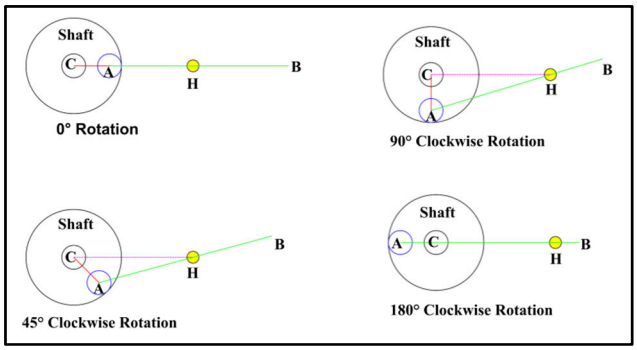

FIGURE 5. Crank slider 3rd inversion.

CA = 15 mm, CH = 50 mm. Diameter of circle A = 10 mm. In 180° Clockwise Rotation,

$$\begin{aligned} \mathrm{AH} &= \mathrm{CA} + \mathrm{CH} \\ \mathrm{AH} &= 65 \text{ mm} \end{aligned} \tag{2}$$

Therefore, AB > 65.

Since at 180° Clockwise Rotation, there is a chance of the green bar slipping out of H(Hinge-slider pin) the length of AB should be greater than 65 mm. The maximum angle between AB at 90-degree clockwise rotation and 270-degree clockwise rotation is 33.4° can be calculated using (3).

$$\begin{aligned} \angle \mathrm{CHA} &= tan^{-1}\left(\frac{CA}{CH}\right) \\ &= tan^{-1}\left(\frac{15}{50}\right) \\ &= 16.69^\circ \end{aligned} \tag{3}$$

The cuttlefish's locomotion for Heave control is achieved by developing VBS (variable buoyancy system) using a Peristaltic motor-powered hydraulic ballast tank in Fig 6, which gives AUV a Variable depth or hover at a certain depth by attaining neutral buoyancy. The VBS is located at the center

of gravity(CG) and inside the main vacuum chamber of the AUV, this minimizes the shift of CG while in operation. The main components of VBS are a piston-ballast tank(45mm OD and 100mm length), a 12v peristaltic DC pump with controller, a limit switch, a Bar300 depth sensor, and a shared 32-bit microcontroller(PID control system).

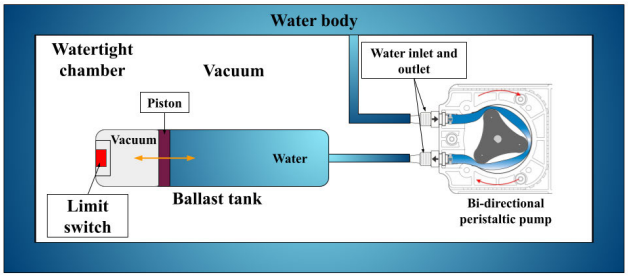

FIGURE 6. Variable buoyancy system.

The prototypes are designed on Fusion 360 software and then manufactured in a fabrication lab. For the first attempt, a 3 mm stainless steel rod is taken and manually folded at consecutive increasing and decreasing 45-degree angles - however, this prototype gives an undesired bent shape when handling rotational torque. In the second attempt, various 3D-printed parts and metal components are assembled to build a crank-shaft structure. This prototype, although worked on a small scale, becomes difficult and expensive to manufacture on a larger scale for the entire AUV vehicle. Ultimately, in the final and third attempt, a single-piece crankshaft with fewer supporting components is manufactured out of aluminium.

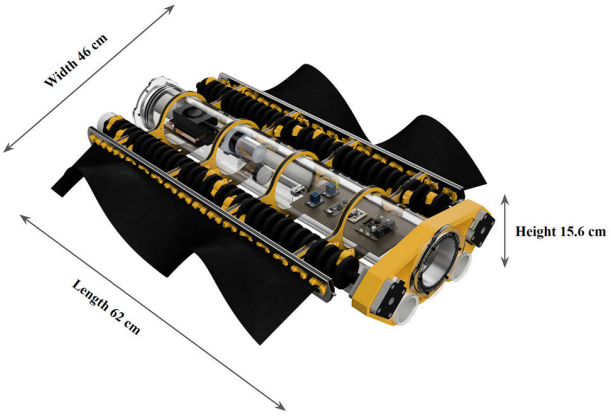

FIGURE 7. Fully assembled prototype CAD design.

Fig 7 displays the prototype of the cuttlefish-inspired autonomous underwater vehicle with its dimensions which weighs 5.5 kg. Fig 8 displays the components of Aquabot.

The main components of Aquabot are as follows:

1. *Sensors:* AUVs use a variety of sensors to collect data, including depth sensors, sonar sensors, temperature sensors, salinity sensors, and imaging sensors. These sensors provide information on the AUV's surroundings, which is used for navigation and data collection. BNO 9 axis IMU sensor is used to navigate the AUV, BAR 30 depth sensor to understand the depth of AUV and IMX219 camera sensor for video sensing.

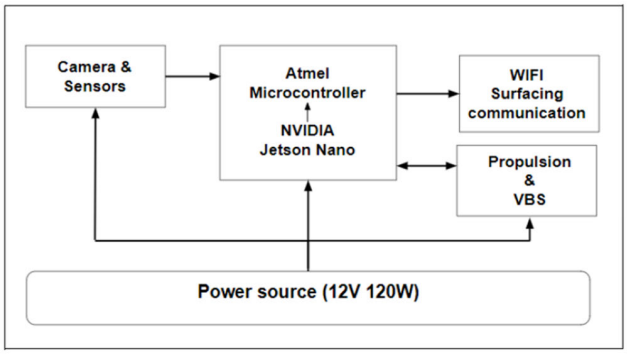

FIGURE 8. Block diagram of Aquabot.

2. *Actuators:* AUVs use actuators to control their movements and perform tasks. These actuators may include thrusters, rudders, and manipulators. In this work, NEMA 17 stepper motor is used as actuator for propulsion system. Stepper motors are not typically designed to work underwater, but parylene coating which is a thin, and transparent polymer coating can provide excellent moisture and chemical resistance to corrosive components of stepper motors for a period. Hence the stator and rotor of stepper motors are coated to protect the stepper motor while submerged in water. This process may degrade motor performance over time and the motor has to be replaced, and it is more economical than using an expensive underwater stepper motor.

3. Control system: The control system is responsible for controlling the AUV's movements based on the data collected from the sensors. It also manages the AUV's power usage and communicates with other components of the AUV. In this work, Arduino Nano Every and Nvidia Jetson Nano are used for deploying the control algorithms and machine learning models. TMC 2208 is the stepper motor driver used for precise motor movement control.

4. Power system: AUVs typically use batteries to power their systems. The power system manages the battery usage to ensure that the AUV has sufficient power to complete its mission. 12 V, 10 Ah Li-Ion batteries of each cell having capacity of 3.6 V is used for power supply.

5. Communication system: AUVs use a communication system to send and receive data, commands, and status updates. This system may communicate with other underwater devices or surface vessels using acoustic or optical communication.

6. Data processing system: AUVs use a data processing system to process the data collected from the sensors. This system may include onboard computers, software, and algorithms that analyse the data and make decisions based on it. Nvidia Jetson Nano is used for data processing control boards.

The mechanical parts of the Aquabot are as follows:

Vacuum control chamber, front and rear seal coupling, seal gaskets, sealing flange, battery housing chamber, split bush, supporting frames for stepper motor in front and middle, split bush, conrod bearings, sliding rod, cylindrical fin support, split hinge, stepper motor, crankshaft assembly, rubber flexible fins, drive end coupling. The mechanical parts of the system are provided in Fig 9.

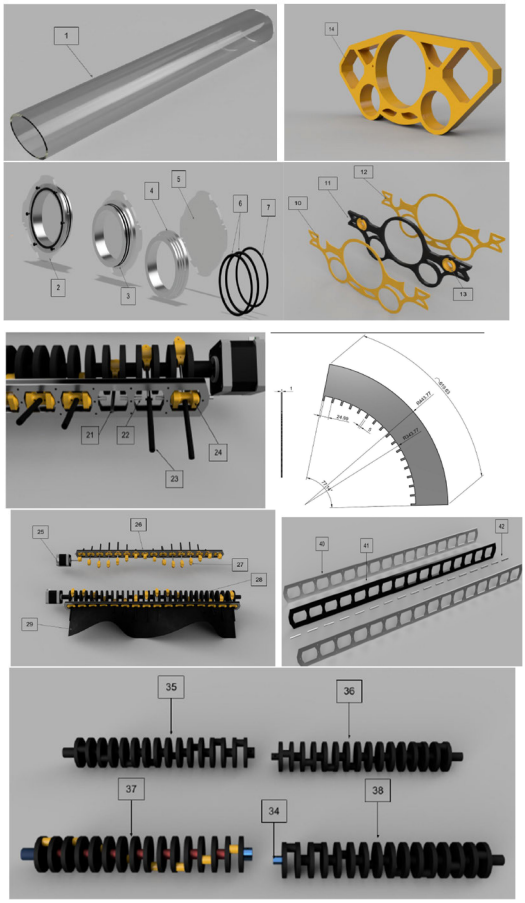

FIGURE 9. Mechanical parts of proposed Aquabot AUV.

The control system of an autonomous underwater vehicle is responsible for the navigation, guidance, and operation of the vehicle. It consists of several components and algorithms that work together to ensure the AUV operates effectively and autonomously, as shown in Fig 10. AUVs are equipped with various sensors to perceive their environment. Common sensors include sonar, cameras, depth sensors, compasses, and Inertial Measurement Units (IMUs). These sensors provide data on the AUV's position, orientation, depth, and surroundings. AUVs use localization algorithms to estimate their position and orientation relative to a reference frame. Simultaneous Localization and Mapping (SLAM) techniques are often employed to create a map of the environment while localizing the AUV within it. Control algorithms translate the desired path into actuator commands, controlling the AUV's thrusters, fins, or other control surfaces to achieve the desired motion. Feedback control loops continuously adjust the vehicle's trajectory based on sensor measurements. AUVs need to detect and avoid obstacles in their path to ensure safe operation. Sensor data, such as sonar readings or visual data, is processed to identify obstacles and collision avoidance algorithms are employed to modify the AUV's path accordingly. The three different PID controls in the control system are the yaw control loop, speed control loop, and depth control loop.

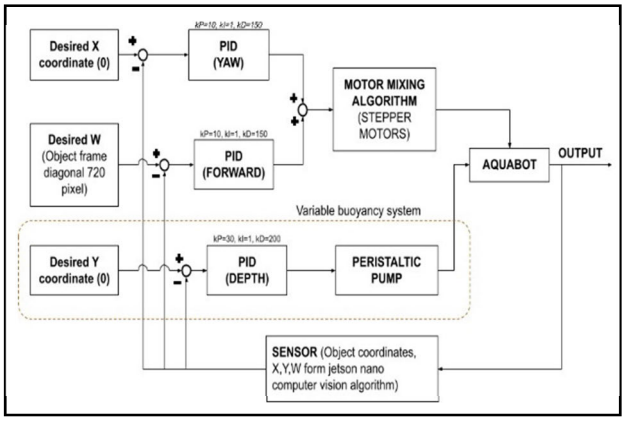

FIGURE 10. Control system of proposed AUV.

IV. PROTOYPING OF PROPOSED AUV

The prototyping of the proposed model is designed where all the parts of the crankshaft is printed in SLA and FDM 3D printers with various materials like PLA and resin for better strength and low friction between dynamic contacts. All support structures are designed and manufactured using CNC laser cutting machine with materials like 1mm thick stainless steel and aluminum sheet and 3D printed PLA parts to reduce the weight. Further to increase the buoyancy, PVC tubes are added that houses the battery system. The major difficulty in this phase of prototyping is making fins for propulsion made using silicon moulding which further increases cost and time. When investigated with various designs of rubber sheet-based cutouts, the fins are assembled using 2 mm screws and staplers which are cheap and durable and the prototyping parts are shown in Fig 11. All the water-sensitive components of AUV is completely sealed inside the vacuum control chamber.

The fully assembled AUV Aquabot has a total weight of 5.5 kg and a total volume of water displaced by AUV is 5420 cubic cm, which gives a net buoyancy of +0.08 kg and is shown in Fig 12.

The basic specifications of Aquabot have been shown in Table 1. The developed Aquabot under water testing is shown in Fig 13.

V. AI-BASED OBJECT DETECTION

The Aquabot is implemented with intelligent AI based object detection which comprises of video enhancement technique

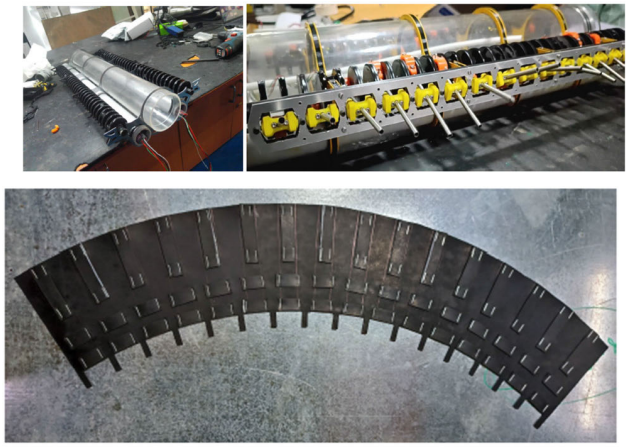

FIGURE 11. Prototyping of assembly parts.

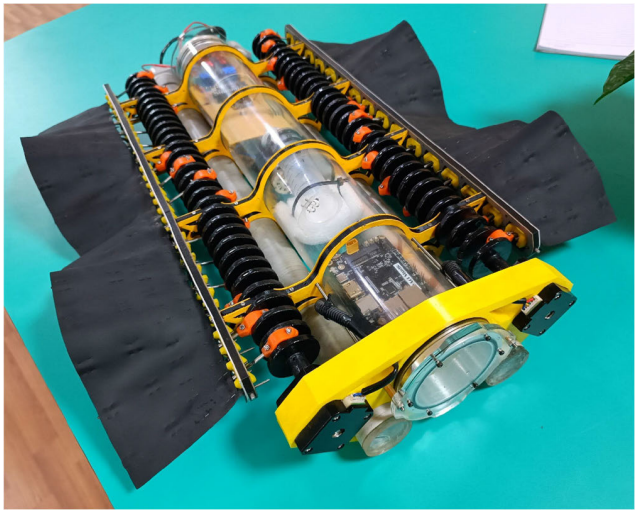

FIGURE 12. Developed Aquabot photograph.

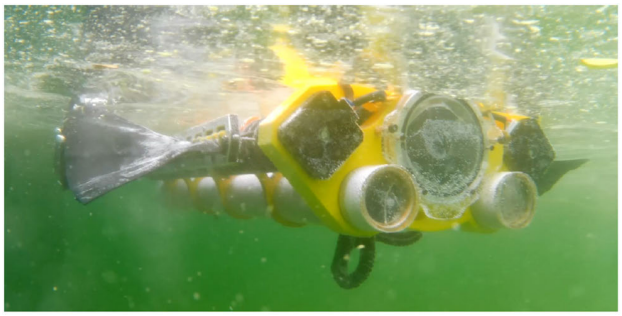

FIGURE 13. Aquabot AUV under wet test.

and object detection. Before doing the accurate bounding box based object detection, the proposed system consists of the following models: (a) Global histogram stretching, b) image histogram division and Rayleigh distribution, c) Gaussian and Laplacian Pyramid, d) Gamma correction, e) video enhancement and f) bounding box using Yolo V5.

TABLE 1. Specifications of AUV Aquabot.

Components	Weight
Weight	5.5 Kg
Net Buoyancy	+0.08 Kg
Dimensions	650 * 460 * 100 nm
Max. Speed	0.2 m/ s
Max Depth	150 m

A. GLOBAL HISTOGRAM STRETCHING

To disperse the pixel values of the picture, the image representation of the multichannel histogram is stretched which implies that it is extended throughout the entire dynamic range of [0, 255]. This prepares the scene for the subsequent step, which divides the histogram into two halves depending on average value. In order to produce a more accurate average of each channel, reflecting the average value of each channel across the whole dynamic range, the stretched-histogram will offer a better pixel distribution of the picture channel. The histogram of the relevant colour band is expanded to include the complete dynamic range using the method described below.

$$P_{\text{out}} = (P_{\text{in}} - \text{i}_{\text{min}}) \left(\frac{O_{max} - O_{min}}{i_{max} - i_{min}} \right) + \text{O}_{\text{min}} \qquad (4)$$

The minimum and maximum intensity level values for the input and output images, respectively, are i_{min}, i_{max}, O_{min}, and O_{max}. P_{in} and P_{out} are the input and output pixels, respectively.

B. IMAGE HISTOGRAM DIVISION AND STRETCHING REGARDING RAYLEIGH DISTRIBUTION

The histogram is divided into two halves using this average value. The histogram is divided into upper and lower halves by dividing it at its average position. The bottom area should have a brightness range between 0 and the mean of the image's histogram, whereas the top part must have a brightness range between the average value and the highest possible intensity range of 255. Stretching 40 these two histogram parts individually in the subsequent step will result in two different histograms. After this step, stretching these regions to follow the Rayleigh pattern across the whole variable range of [0, 255] occurs. The bottom region will be enlarged to include the entire dynamic range of [0, 255] if the intensity value of the bottom area is between 0 and the average value. The same method is used to extend the initial range of the top area, which goes from the average value to 255, to include the entire dynamic range of [0, 255]. Equation 5 yields the Rayleigh distribution's probability distribution function.

$$\text{PDF}_{\text{Rayleigh}} = \left(\frac{x}{\alpha^2} \right) e^{\left(\frac{-x^2}{2\alpha^2} \right)} \quad \text{for } \text{x} \geq 0, \alpha \succ 0 \qquad (5)$$

where x is the input data, in this case the intensity value, and is the Rayleigh distribution's distribution parameter.

Rayleigh-stretched distribution in (6):

$$\text{Rayl}_{\text{stretched}} = \frac{\left[(P_{in} - i_{min})\left(\frac{O_{max}-O_{min}}{i_{max}-i_{min}}\right) + O_{min}\right]}{\alpha^2} .e^{\frac{-\left[(P_{in}-i_{min})\left(\frac{O_{max}-O_{min}}{i_{max}-i_{min}}\right)+O_{min}\right]^2}{2\alpha^2}} \quad (6)$$

The produced histogram spans the complete [0, 255] dynamic range. Therefore, 255 and 0, respectively, can be used as substitutes for the values of O_{max} and O_{min}. As a result, (6) may be simplified as follows:

$$\text{Rayl}_{\text{stretched}} = \frac{255\,(P_{in} - i_{min})}{\alpha^2\,(i_{max} - i_{min})} .e^{\frac{-[255(P_{in}-i_{min})]^2}{2\alpha^2(i_{max}-i_{min})^2}} \quad (7)$$

C. GAUSSIAN AND LAPLACIAN PYRAMID

A multi-scale representation of a picture may be created using the Gaussian Pyramid approach. It comprises two steps:

(1) smoothing to eliminate any potential high-frequency components. Reduce the image size in half through smoothing, also known as blurring, aliasing, and down-sampling. Laplacian Pyramid is a method of computing and storing the difference between each level.

In addition to recovering lost frequencies, Laplacian Pyramid also eliminates the necessity to keep smoothed pictures in Gaussian Pyramid for the duration of its storage.

VI. PROPOSED VIDEO ENHANCEMENT MODEL

The process involves extracting individual frames from a video, enhancing them using image enhancement techniques, and then combining them back together to create a new and improved video. The first step in this process is to extract the frames from the video. This can be done using software that can split the video into individual frames. Once the frames are extracted, they can be analyzed and enhanced using various image enhancement techniques such as noise reduction, contrast enhancement, and color balance adjustment. These techniques can be applied to each frame individually or to multiple frames simultaneously to improve the consistency of the enhancements across the video. After the frames have been enhanced, they are combined back together to create a new and improved video. This can be done using software that can merge the frames together to form a new video. However, the benefits of using this technique can be significant, especially for videos that have poor visual quality due to factors such as low lighting or poor camera quality. Object detection models are classified into two types: two-stage object detectors and single-stage object detectors. To create dense predictions, single-stage object detector architectures (such as YOLO) are built of three components backbone, neck, and head, as illustrated in the image below. The backbone is a pre-trained network that is used to generate picture rich feature representations. This aids in reducing the image's spatial result while boosting its feature (channel) resolution. YOLOv5 measures the features of the maps utilising the CSPNet process of the base layer into two parts and then merges them through with a cross-stage hierarchy.

First, a variant of Spatial Pyramid Pooling (SPP) was utilised, and the Path Aggregation Network (PANet) was unique as it contained the BottleNeckCSP in its architecture as shown in Fig 14. PANet is a feature pyramid network that was utilised in later versions of YOLO (YOLOv4) to enhance information flow and aid in the accurate localization of pixels in the mask prediction job. This network has been modified in YOLOv5 by employing the CSPNet technique. The SPP blocks aggregates the information from the inputs and provides a fixed length output. As a result, it has the benefit of considerably extending the receptive field and isolating the YOLO algorithm which works using following three techniques: 1) Bounding Box Regression, 2) Intersection Over Union, 3) Residual Blocks (IOU).

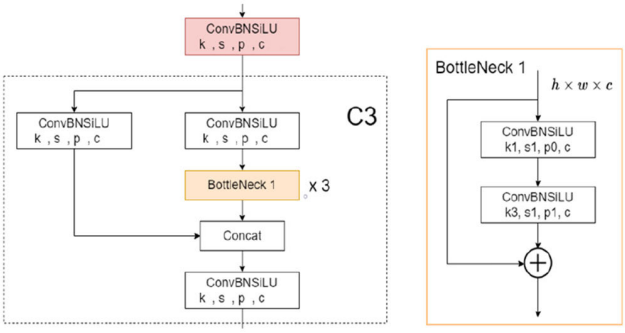

FIGURE 14. Yolo V5 algorithm.

The image is initially divided into several grids. Each column have a dimension of S x S. Grids made from a commentary picture. In the picture above, there are actually numerous grid cells with appropriate size. Each grid cell will be capable of detecting things that enter it. A grid cell, for example, will be responsible for identifying an object if its centerfield occurs within that cell. Most relevant context information while maintaining network speed.

A bounding box as shown in Fig 15 represents a compression that draws focus on a feature in an image. Each bounding box in the picture has the following characteristics: Height (bh), width (bw), class (for example, fish, diver, etc.) is signified by the letter, Bounding box middle (bx,by).The picture beneath is a depiction for a bounding box. The box's arrival is characterised by an object recognition phenomena known as IOU. YOLO use the IOU to generate an output box that suitably surrounds objects. Each pixel of the grid has responsibility for the forecast box boundaries with their associated confidence values. The IOU is 1 if the anticipated boundary box and the actual box match. This hit discards bounding boxes that do not match the actual box. The depression in the visual shows a simple IOU process. The green area reflects the actual area, while the red area represents the estimated field.

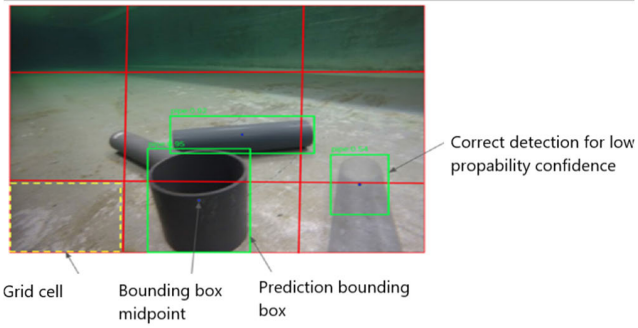

FIGURE 15. Bounding box of object detection module.

VII. RESULTS AND DISCUSSION

A. ANALYSIS OF FUSION 360 AND ANSYS

The 3D models are analyzed before manufacturing using Fusion 360 simulation and Ansys Software. The stress analysis tools in Fusion 360 use Finite Element Analysis (FEA) to simulate the behaviour of the structure whereas ANSYS Fluent is a popular software tool used for Computational Fluid Dynamics (CFD) analysis. CFD analysis allows engineers to simulate the behaviour of fluids and gases in real-world scenarios, including aerodynamics, thermodynamics, and hydrodynamics. Some of the results of the above analysis are shown below, Fig 16 shows the main element of propulsion i.e. crankshaft has a displacement of 0.25 mm which gives a very high safety factor of 8. Fig 17 shows the safety factor of crankshaft and Fig 18 depicts the fluid turbulence contour of AUV.

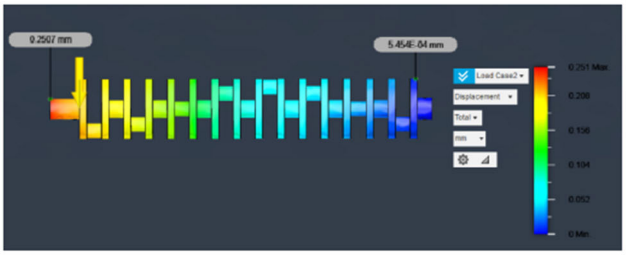

FIGURE 16. Displacement factor of crankshaft.

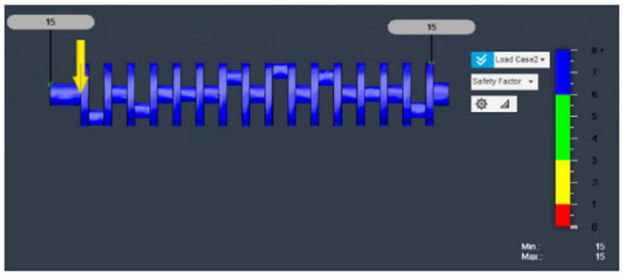

FIGURE 17. Safety factor of crankshaft.

B. FIELD TEST RESULTS

The resistance force, RPM and power due to velocity has been recorded during field test are shown in Table 2 and Fig 19. The highest resistance of 6.8 N at max velocity of 0.2 m/s has been recorded. The peak power consumption is 36 at a max velocity of 0.2 m/s.

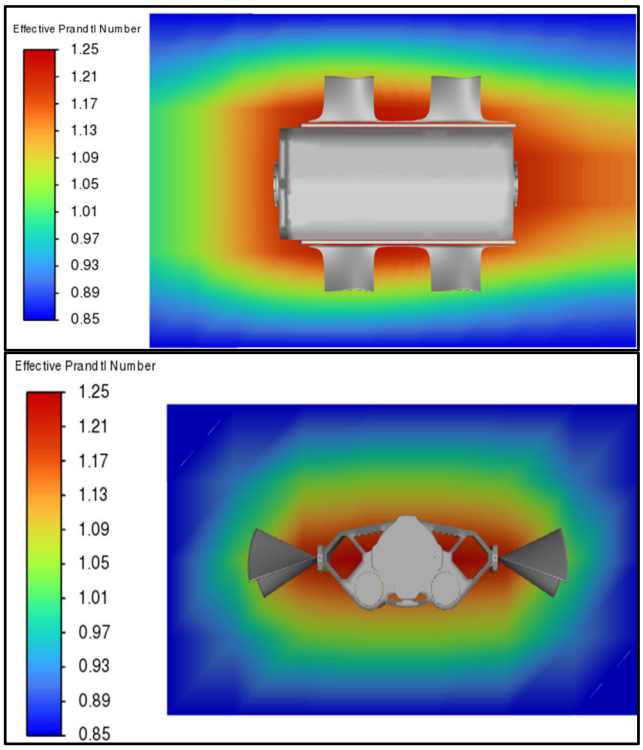

FIGURE 18. Fluid turbulence contour around AUV (top view) and (front view).

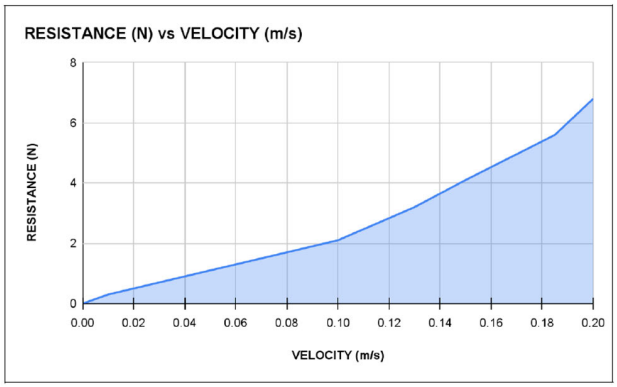

FIGURE 19. Resistance(N) vs Velocity(m/s) graph.

The maximum power consumption of AUV Aquabot is shown in Table 3. The battery has a capacity of 10 Ah, and the maximum current consumption during the field test is 3 A. So this gives the endurance of more than 3 hr at extreme testing conditions.

The plots of velocity versus RPM and Power versus RPM are shown in Fig 20 and 21, respectively.

C. RESULTS ON UNDERWATER IMAGE ENHANCEMENT AND OBJECT DETECTION

A thorough analysis of both real-time and unreal-time advancements in underwater image processing was

TABLE 2. Resistance due to velocity.

Power (W)	Resistance (N)	RPM	Velocity (m/s)
15.6	0	0	0
16.8	0.3	20	0.01
17.4	0.7	40	0.03
18	1.3	60	0.06
18.36	2.1	80	0.1
22.44	3.2	100	0.13
25.2	4.1	120	0.15
30	5.6	140	0.185
36	6.8	160	0.2

TABLE 3. Maximum power consumption of AUV.

S. No	Components	Power Consumption (max)
1	Stepper Motor	18 W
2	Jetson Nano (Microprocessor)	12 W
3	Buoyancy System	1.6 W
4	Other sensors and microcontroller	0.8 W
	TOTAL	32. 4 W

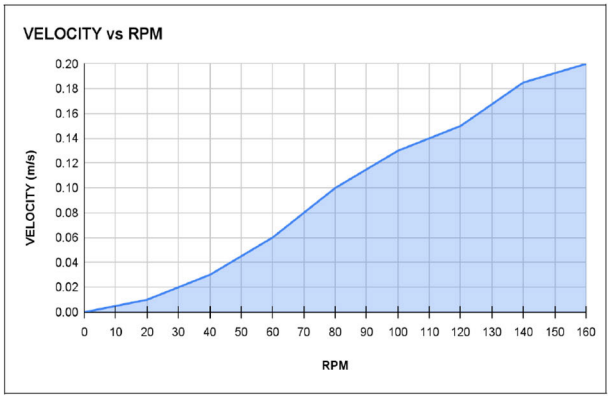

FIGURE 20. Velocity (m/s) VS RPM.

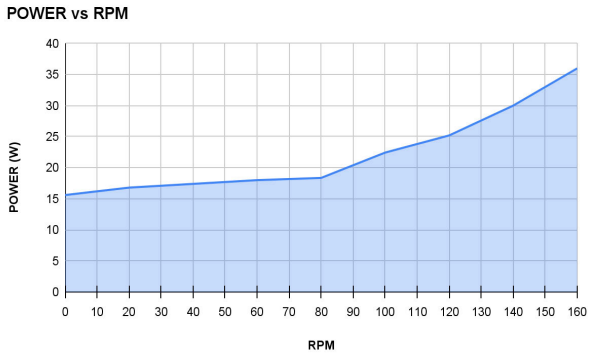

FIGURE 21. Power (W) VS RPM.

developed and different sorts of the direction of the potential best image quality are explored depending on the various states of water, their depths, and their variable levels as shown in Fig 22. These real-time images show the or near real-time techniques consist of five primary image processing-based phases. These five phases include color space conversion, noise reduction, blurring removal, contrast improvement of the underwater picture using histogram equalization and stretching, wavelet transformation, and image restoration and is shown in Fig 23. Each method has been used to enhance the caliber of underwater photos in specific categories. By integrating them or making better use of the solutions. With a sensor size of 3.674 × 2.760 mm, the IMX 219 camera capture detailed images and videos in this work. The proposed work mainly concentrates in the video enhancement, image sharpness enhancement. The dataset for object detection includes different type of animal species coral, crab, fish, goldfish, jellyfish, lobster, octopus, oysters, rock, seal, snail, snake, squid, starfish, turtle and other than aquatic creatures our dataset also includes the rocks and the divers for further clarity.

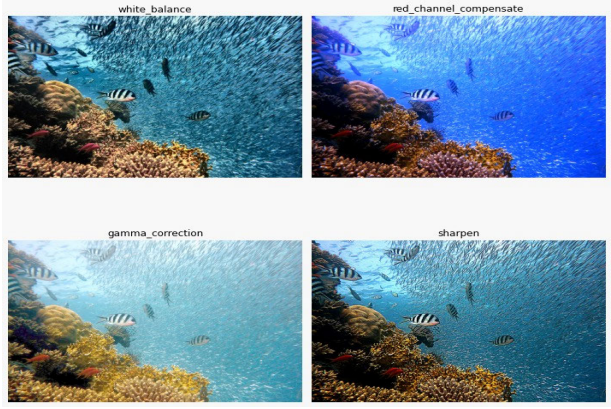

FIGURE 22. Processing of underwater images.

Images have been collected during the research, some of them are snipped from the video frames, and some are the random data collected individually from the browser. To attain a full-fledged dataset and to get an accurate detection when we run it on random pictures and videos, we can achieve the desired accuracy. All the images in the dataset are trained, labelled, and tested with the help of external software. After this process the images are exported with the help of an API key given by the that software. the API key have to be added in the code along yolo v5 code so that our code can be easily train the images and we can achieve our desired output.

Table 4 provides the MAP score for different Yolo models tried for object detection. The maximum performance is achieved by training the second dataset on Yolo V5 model.

Multiple field tests are performed after aggregating all components together – resulting in successful vehicle navigation using AI, hence validating the proposed autonomous nature of our AUV. Finally, the AUV Aquabot prototype is fully configured to execute autonomous operations in the ocean and aquafarm. From the broad to the specific, this work has progressed from the fundamentals of computer vision to how and why to distinguish things, how it enhances images,

(a) Before image enhancement

(b) After proposed image enhancement

FIGURE 23. Different stages of image correction.

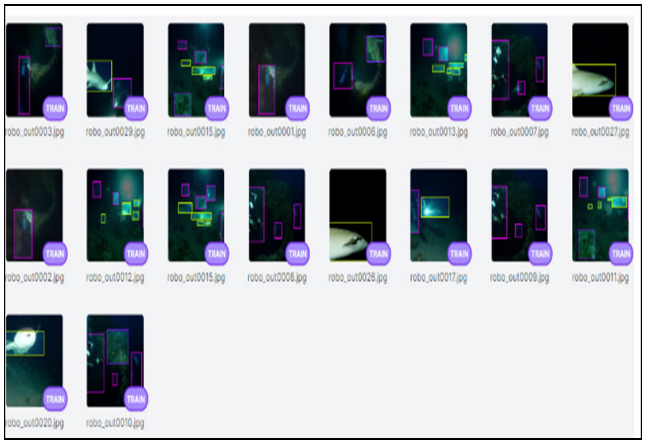

FIGURE 24. Enhanced images using proposed model.

TABLE 4. MAP score comparison for object detection models.

S. No	Model Type	MAP Score
1	YOLO V5 (Resize 640 * 640)	98.6
2	YOLO V5 (Resize 416 * 416)	98.3
3	YOLO V5(Resize 416*416 + Auto Orient)	98.5
4	YOLO V4 tiny	97.4
5	YOLO V6	96.7
6	YOLO V7	97.2

evaluates distance and angle with relation to a camera, and more. shown how individuals may be recognized and tracked using object recognition software for spying and other purposes. The system for object identification, image processing, and angle measurement has a new tool that highlights some of its accomplishments.

VIII. CONCLUSION

The proposed Bio-inspired propulsion system has been designed in Fusion 360 software and models were analysed in Ansys software to verify the strength and manufacturability of components. Then the parts of propulsion are manufactured using 3D printing, Laser cutting and CNC machining process. After assembling all components, the buoyancy and water tightness of the AUV were tested in the underwater environment, and the results were noted to add improvements in the prototype. The electronics, embedded control system and autonomous algorithms have been integrated and deployed in the AUV. In conclusion, utilising YOLOv5 to detect objects in underwater films is a strong and successful technique. Modern deep learning model YOLOv5 is excellent in real-time object detection tasks. The excellent accuracy and quick inference times of YOLOv5's sophisticated architecture make underwater object recognition practical in real-world situations. A broad and representative dataset of annotated underwater photos or videos is first needed for model training. These issues can be overcome by fine-tuning the model using domain-specific underwater data and utilizing preprocessing techniques to improve image quality.

APPENDIX

1- Vacuum control chamber
14- Stepper motor supporting frame
2- Front seal coupling
3- Rear seal coupling
4- O ring sealing flange
5- Enclosure disc
6,7- Seal gasket A and B
10- front support frame dual opening type
11- middle supporting frame
12- rear supporting frame dual opening type
13- Split brush
21- Sliding rod
22- Hinge axial
23- Cylindrical fin support
24- Split Hinge
25- Stepper motor
26- Hinge support frame
27- Split conrod bearing assembly
28- Crankshaft assembly
29- Rubber flexible fin
34- Crankshaft coupling male
35- Crankshaft front clockwise
36- Crankshaft rear clockwise
37- Crankshaft front anti-clockwise
38- Crankshaft rear anti-clockwise
40- Hinge support envelope
41- Hinge support main frame
42- Hinge axial

ACKNOWLEDGMENT

The authors thank Dr. N. Vedachalam and Ms. Bala Naga Jyothi of the National Institute of Ocean Technology (NIOT) for their technical support, and Director, NIOT for his continuous encouragement.

REFERENCES

[1] L. Paull, S. Saeedi, M. Seto, and H. Li, "AUV navigation and localization: A review," *IEEE J. Ocean. Eng.*, vol. 39, no. 1, pp. 131–149, Jan. 2014, doi: 10.1109/JOE.2013.2278891.
[2] J. Hwang, N. Bose, and S. Fan, "AUV adaptive sampling methods: A review," *Appl. Sci.*, vol. 9, no. 15, p. 3145, Aug. 2019.
[3] F. Maurelli, S. Krupiński, X. Xiang, and Y. Petillot, "AUV localisation: A review of passive and active techniques," *Int. J. Intell. Robot. Appl.*, vol. 6, no. 2, pp. 246–269, Jun. 2022.
[4] E. Fiorelli, N. E. Leonard, P. Bhatta, D. A. Paley, R. Bachmayer, and D. M. Fratantoni, "Multi-AUV control and adaptive sampling in Monterey bay," *IEEE J. Ocean. Eng.*, vol. 31, no. 4, pp. 935–948, Oct. 2006.
[5] D. Li and L. Du, "AUV trajectory tracking models and control strategies: A review," *J. Mar. Sci. Eng.*, vol. 9, no. 9, p. 1020, Sep. 2021.
[6] R. Wang, Y. Li, T. Ma, and Y. Chen, "Initial positioning of terrain relative navigation under pseudo-peaks interference," *IEEE Trans. Instrum. Meas.*, vol. 72, pp. 1–16, 2023.
[7] J. G. Jimenez, M. J. Bays, D. J. Stilwell, H. Yetkin, and M. Kim, "Optimizing unmanned underwater vehicle surfacing using a Poisson process," in *Proc. OCEANS MTS/IEEE US Gulf Coast*, 2023, pp. 1–8.
[8] A. Bhardwaj, A. Allam, A. Erturk, and K. G. Sabra, "Ultrasound-powered wireless underwater acoustic identification tags for backscatter communication," *IEEE Trans. Ultrason., Ferroelectr., Freq. Control*, vol. 71, no. 2, pp. 304–313, Feb. 2024.
[9] Y. Liu, Y. Wang, C. Chen, and C. Liu, "Unified underwater acoustic localization and sound speed estimation for an isogradient sound speed profile," *IEEE Sensors J.*, vol. 24, no. 3, pp. 3317–3327, Feb. 2024.
[10] P. Ridao, J. Yuh, J. Batlle, and K. Sugihara, "On AUV control architecture," in *Proc. IEEE/RSJ Int. Conf. Intell. Robots Syst. (IROS)*, vol. 2, 2000, pp. 855–860.
[11] C. Cheng, Q. Sha, B. He, and G. Li, "Path planning and obstacle avoidance for AUV: A review," *Ocean Eng.*, vol. 235, Sep. 2021, Art. no. 109355.
[12] M. Erol, L. F. M. Vieira, and M. Gerla, "AUV-aided localization for underwater sensor networks," in *Proc. Int. Conf. Wireless Algorithms, Syst. Appl. (WASA)*, Aug. 2007, pp. 44–54.
[13] H. Singh, A. Can, R. Eustice, S. Lerner, N. McPhee, and C. Roman, "Seabed AUV offers new platform for high-resolution imaging," *Eos, Trans. Amer. Geophys. Union*, vol. 85, no. 31, pp. 289–296, Aug. 2004.
[14] M. B. Loc, H.-S. Choi, J.-M. Seo, S.-H. Baek, and J.-Y. Kim, "Development and control of a new AUV platform," *Int. J. Control, Autom. Syst.*, vol. 12, no. 4, pp. 886–894, Aug. 2014.
[15] S. Licht, V. Polidoro, M. Flores, F. S. Hover, and M. S. Triantafyllou, "Design and projected performance of a flapping foil AUV," *IEEE J. Ocean. Eng.*, vol. 29, no. 3, pp. 786–794, Jul. 2004.
[16] B. Allotta, A. Caiti, R. Costanzi, F. Fanelli, D. Fenucci, E. Meli, and A. Ridolfi, "A new AUV navigation system exploiting unscented Kalman filter," *Ocean Eng.*, vol. 113, pp. 121–132, Feb. 2016.
[17] S. Tangirala and J. Dzielski, "A variable buoyancy control system for a large AUV," *IEEE J. Ocean. Eng.*, vol. 32, no. 4, pp. 762–771, 2007.
[18] R. McEwen, H. Thomas, D. Weber, and F. Psota, "Performance of an AUV navigation system at Arctic latitudes," *IEEE J. Ocean. Eng.*, vol. 30, no. 2, pp. 443–454, Apr. 2005.
[19] D. Ribas, P. Ridao, A. Turetta, C. Melchiorri, G. Palli, J. J. Fernández, and P. J. Sanz, "I-AUV mechatronics integration for the TRIDENT FP7 project," *IEEE/ASME Trans. Mechatronics*, vol. 20, no. 5, pp. 2583–2592, Oct. 2015.
[20] C. McGann, F. Py, K. Rajan, H. Thomas, R. Henthorn, and R. McEwen, "A deliberative architecture for AUV control," in *Proc. IEEE Int. Conf. Robot. Autom.*, May 2008, pp. 1049–1054.
[21] V. Upadhyay, S. Gupta, A. C. Dubey, M. J. Rao, P. Siddhartha, V. Gupta, S. George, R. Bobba, R. Sirikonda, A. Maloo, and V. G. Idichandy, "Design and motion control of autonomous underwater vehicle, amogh," in *Proc. IEEE Underwater Technol. (UT)*, Chennai, India, Feb. 2015, pp. 1–9.
[22] B. Aktas, M. Atlar, S. Turkmen, W. Shi, R. Sampson, E. Korkut, and P. Fitzsimmons, "Propeller cavitation noise investigations of a research vessel using medium size cavitation tunnel tests and full-scale trials," *Ocean Eng.*, vol. 120, pp. 122–135, Jul. 2016.
[23] M. A. Kolmann and A. P. Summers, "Sharks shift their spine into high gear," *Nature*, vol. 540, no. 7634, pp. 532–533, Dec. 2016.
[24] M. Saad, S. A. Khan, M. H. Ahmad, S. S. H. Zaidi, Z. Riaz, S. Ahmed, and R. Khan, "Modeling and simulation of electric propulsion system for UUVs to observe variations in drag and Motor's power against operational and design parameters using MATLAB," in *Proc. 17th Int. Bhurban Conf. Appl. Sci. Technol. (IBCAST)*, Jan. 2020, doi: 10.1109/IBCAST47879.2020.9044542.
[25] J. F. Carneiro, J. B. Pinto, F. G. de Almeida, and N. Cruz, "Using a variable buoyancy system for energy savings in an AUV," in *Proc. 5th Exp. Int. Conf. (Exp. At)*, Funchal, Portugal, Jun. 2019, pp. 305–309.
[26] F. Plum, S. Labisch, and J.-H. Dirks, "SAUV—A bio-inspired soft-robotic autonomous underwater vehicle," *Frontiers Neurorobotics*, vol. 14, p. 8, Feb. 2020.
[27] A. Ayob, F. Khairuddin, Y. M. Mustafa, A. R. Salisa, and K. Kadir, "Analysis of pruned neural networks (MobileNetV2-YOLO v2) for underwater object detection," in *Proc. 11th Nat. Tech. Seminar Unmanned Syst. Technol.* Singapore: Springer, 2021, pp. 1–12.
[28] D. Thuan. (2021). *Evolution of YOLO Algorithm and YOLOv5: The State-of-the-Art Object Detention Algorithm*. [Online]. Available: https://www.theseus.fi/handle/10024/452552
[29] W. Xu and S. Matzner, "Underwater fish detection using deep learning for water power applications," in *Proc. Int. Conf. Comput. Sci. Comput. Intell. (CSCI)*, Las Vegas, NV, USA, Dec. 2018, pp. 313–318.
[30] M. Yang and A. Sowmya, "An underwater color image quality evaluation metric," *IEEE Trans. Image Process.*, vol. 24, no. 12, pp. 6062–6071, Dec. 2015.
[31] Y.-T. Kim, "Contrast enhancement using brightness preserving bi-histogram equalization," *IEEE Trans. Consum. Electron.*, vol. 43, no. 1, pp. 1–8, Feb. 1997.
[32] J. Redmon, S. Divvala, R. Girshick, and A. Farhadi, "You only look once: Unified, real-time object detection," in *Proc. IEEE Conf. Comput. Vis. Pattern Recognit. (CVPR)*, Las Vegas, NV, USA, Jun. 2016, pp. 779–788.

ARYAN ANAND (Member, IEEE) received the bachelor's degree in electrical and electronics engineering from SRM University, Chennai, India, in July 2023, with a focus on embedded system design, automation, control systems, marine robotics, CAD design, and project management. He is currently pursuing the master's degree in electrical engineering with The University of Texas at Tyler. He serves as a Graduate Research Assistant under Dr. Prabha Sundaravadivel. He engaged in projects centered around autonomous robots for agriculture and aquaculture, as well as an AI-powered instrumental setup for fish behavior recognition, he collaborates with well-known research firms. His notable achievements include automating a prestigious laboratory at SRM University, developing a patent-pending bio-inspired autonomous underwater vehicle, and serving as the Chair for the SRM-MTS Students Chapter. He has been recognized with two awards at Oceans 2022 conferences, such as the IEEE SPF Madras Section, in 2022, and the Best Project Award from SRMIST, in 2023.

M YUVA BHARATH received the Diploma degree in electrical and electronics engineering from Vickram Polytechnic College and the B.Tech. degree in electrical and electronics engineering from the SRM Institute of Science and Technology. He was the Vice President of the SRM MTS Student Chapter. He did an internship with the National Institute of Ocean Technology (NIOT) for the development of AUV control systems and docking. He is currently a Research and Development Engineer with Electric Mobility startup companies, such as AR4 Tech Pvt. Ltd. and Weber Mobility AB. He is also working on sodium ion battery pack technology for energy storage applications and electric vehicles. His research interests include low-speed electric scooters, sodium-ion battery packs for LCV, and renewable energy storage systems with sodium-ion technology.

PRABHA SUNDARAVADIVEL (Member, IEEE) received the B.Tech. degree in electronics and communication engineering from the SRM Institute of Science and Technology, Kattankulathur, India, in 2011, the M.Tech. degree in VLSI design from VIT University, Vellore, India, in 2015, and the Ph.D. degree in computer science and engineering from the University of North Texas, Denton, TX, USA, in 2018.

She is currently the Director of the Center for Robotics and Intelligent Systems (CeRIS), The University of Texas at Tyler. Her research interests include developing application-specific architectures for smart healthcare and smart cities, sustainable cyber-physical systems, edge-intelligent embedded systems for the IoT applications, reconfigurable computing, bio-inspired robotics, and applied machine learning. She received the Outstanding Early Career Researcher Award from the IEEE Bio-Inspired Computing, in 2022, and the Teaching and Learning Award for introducing innovative teaching techniques in the undergraduate curriculum, in 2019. She has also been recognized as a Faculty Scholar in the Grace Hopper Celebration of Women in Computing, in 2019, and the ACM Richard Tapia Conference for Celebration of Diversity in Computing, in 2022.

J. PREETHA ROSELYN (Senior Member, IEEE) received the B.E. degree in electrical and electronics engineering from Madras University, India, in 2002, the M.S. degree (by Research) in power systems from Anna University, Chennai, and the Ph.D. degree from SRM University, India. She is currently a Professor with the Department of Electrical and Electronics Engineering, SRM Institute of Science and Technology, India. She has published 50 international publications, including 25 SCI-indexed journals, four lecture notes, 25 conference publications, and a book. She has received government-funded projects from DST, India; MoES, India; and AICTE, India. Her research interests include power system stability, digital twins, intelligent controllers for microgrids, and power system security. She is acting as the Chairperson of the MTS India Section and the Branch Councilor of the SRM MTS Student Chapter. The chapter has received the Best Student Chapter Award for the year 2019. She was also a recipient of the John P. Craven Mentor Award, in 2022.

R. ANNIE UTHRA received the B.E. degree in computer science and engineering from Manonmaniam Sundaranar University, India, and the M.S. and Ph.D. degrees from SRM University, Chennai, India. From 2012 to 2018, she was an Adjunct Associate Teaching Professor with the Institute for Software Research, School of Computer Science, Carnegie Mellon University, Pittsburgh, PA, USA. From 2018 to 2020, she was a Visiting Professor with Henan University of Economics and Law, Zhengzhou, Henan, China. She is currently a Professor and the Head of the Computational Intelligence Department, SRM Institute of Technology. Her scholarly and teaching interests include wireless sensor networks, machine learning, positioning and navigation, the IoT, and energy-aware routing techniques. She was a recipient of the IET CLN Women Engineer, from 2016 to 2017, the Outstanding Reviewer Award from the *Journal of Network and Computer Applications* (Elsevier), and the Best Teacher Award, in 2006.